Letter

Braiding topology of symmetry-protected degeneracy points in non-Hermitian systems

Jia-Zheng Li,[1] Kai Bai,[1] Cheng Guo,[2] Tian-Rui Liu,[1] Liang Fang,[1] Duanduan Wan,[1,*] and Meng Xiao[1,3,†]

[1]*Key Laboratory of Artificial Micro and Nanostructures of Ministry of Education and School of Physics and Technology, Wuhan University, Wuhan 430072, China*

[2]*Department of Applied Physics, Stanford University, Stanford, California 94305, USA*

[3]*Wuhan Institute of Quantum Technology, Wuhan 430206, China*

(Received 27 September 2023; revised 13 December 2023; accepted 14 December 2023; published 5 January 2024)

Degeneracy points in non-Hermitian systems are of great interest. While a homotopic framework exists for understanding their behavior in the absence of symmetry, it does not apply to symmetry-protected degeneracy points with reduced codimension. In this work, utilizing algebraic topology, we provide a systematic classification of these symmetry-protected degenerate points and investigate the braid conservation rule followed by them. Using a model Hamiltonian and circuit simulation, we discover that, contrary to simple annihilation, pairwise-created symmetry-protected degeneracy points merge into a higher-order degeneracy point, which goes beyond the abelian picture. Our findings empower researchers across diverse fields to uncover new phenomena and applications harnessing symmetry-protected non-Hermitian degeneracy points.

DOI: 10.1103/PhysRevB.109.L041102

Introduction. Band degeneracies have played a significant role in the topological band theory of Hermitian systems, with their topology classified through homotopy theory [1–3]. Well-known instances, such as Weyl points, Dirac points, and nodal lines [4–8], led to a plethora of exotic physics [9–15]. In recent years, the study of non-Hermitian systems has gained momentum [16–22]. In non-Hermitian settings, degeneracies can possess complex values and encompass more exotic singularities, such as defective degeneracies known as exceptional points [23–25], as well as unique nondefective degeneracy points that do not have counterparts in the Hermitian regime [22,26,27]. Recent investigations have revealed that non-Hermitian degeneracies without any symmetry can be classified by the braid group $\mathcal{B}_n$ [28,29], which goes beyond the topological classification based on line or point gaps [16,17]. Since $\mathcal{B}_n$ is a nonabelian group for $n \geqslant 3$ where n is the dimension of a Hamiltonian, the evolution of non-Hermitian degeneracies follows a nonabelian conservation rule (NACR) [30–32]. Braided structures in Hermitian systems have led to many exotic phenomena [1,14,33–39]. Consequently, the recent discovery of braid topology in non-Hermitian systems without symmetry has further sparked exploration in various fields including acoustics [40,41], photonics [21], and condensed matter physics [42].

Symmetry plays a vital role in topological phases. In Hermitian systems, the ten-fold Altland-Zirnbauer symmetry [43] unlocks the classification of symmetry-protected topological phases beyond the scenarios without any symmetry. Similarly, in non-Hermitian systems, 38-fold symmetry enriches the classifications of wave-function topology based on K-theory [16,19]. Symmetries also have important consequences in the braid properties of spectral topology in non-Hermitian systems. Of particular importance are symmetries that can reduce the codimension of degeneracy points, such as pseudo-Hermiticity (psH), parity-time symmetry (PT), chiral symmetry (CS), and parity-particle-hole symmetry (CP) [22–24,26,44–53]. Such symmetries can significantly affect the braid topology. Specifically, for a system without symmetry, the generic degeneracy point has codimension 2 and thus occurs as a isolated point in a two-dimensional (2D) parameter space [the left panel of Fig. 1(a)]. The topology of such a point can be characterized by the closed path encircling it, based on the homotopy theory. However, with the above symmetries, the generic degeneracy has codimension 1 [45,54] and thus forms a nodal line in a 2D parameter space [the right panel of Fig. 1(a)]. Consequently, its topology can no longer be characterized by a closed path as the path would unavoidably cross the singularities [53,55], disallowed in homotopy theory [28–30,53,56]. As a result, the braid topology classifying degeneracy points in non-Hermitian systems with symmetry remains elusive.

In this work, we address this question by providing a general theory to elucidate the braid topology associated with symmetry-protected degeneracy points. We demonstrate that, in the situation with reduced codimension, the eigenvalue topology can be characterized by the braid group $\mathcal{B}_m$, where m is no longer the dimension of the system Hamiltonian. Furthermore, a specific type of degeneracy points, distinct from the ordinary degeneracy points in systems without symmetry, contributes to the braid topology. Additionally, a NACR governs the parametric evolution of these degeneracy points. We illustrate this NACR with exemplary systems. Our work not only extends the scope of the braid topology to non-Hermitian systems with symmetries, but also enables researchers to harness and manipulate these symmetry-protected degeneracy points in various physical domains, such as circuit systems [49–51,57], acoustic cavities [40,41], and coupled ring resonators [23,52,58].

*ddwan@whu.edu.cn

†phmxiao@whu.edu.cn

 ©2024 American Physical Society

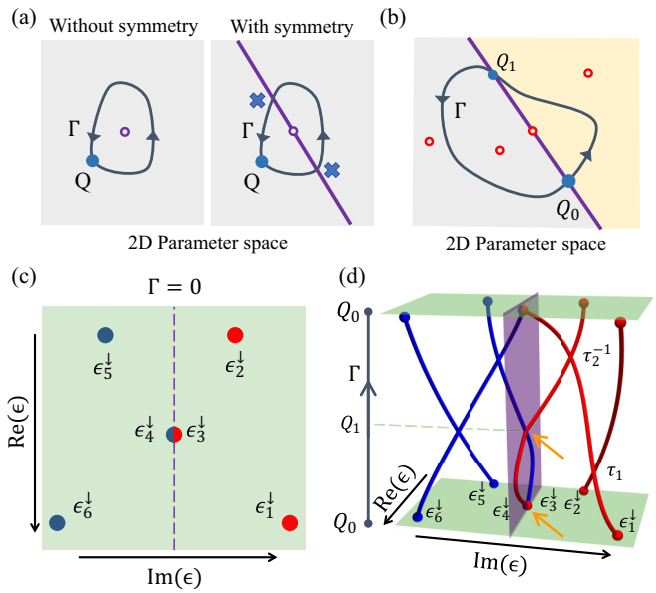

FIG. 1. (a) A degeneracy point (the purple circle in the left panel) without symmetry becomes a nodal line (the purple line in the right panel) in the presence of certain symmetries. (b) A closed path (the blue-black arrowed line) originating from Q_0 enclosing two CPDPs (red circles) and passing through a nodal line in a 2D parameter space. This nodal line separates two areas (beige and gray) with probably different numbers of complex conjugate pairs of eigenvalues. (c) An illustration of sorting eigenvalues of a 6×6 non-Hermitian system with PT or psH symmetry at the beginning of the path Γ. (d) An illustration of braiding of the eigenvalue strands along the path Γ in (b). τ_i denotes the braid algebra.

Theory. We introduce the notations used in this Letter. $\mathbb{Z}$, $\mathbb{R}$, $\mathbb{R}_+$, and $\mathbb{C}$ denote the sets of integers, real numbers, nonnegative real numbers, and complex numbers, respectively. $\mathbb{C}_{+(-)} = \{x \in \mathbb{C} \mid \mathrm{Im}(x) \geqslant (\leqslant) 0\}$ while $\mathbb{C}_+^0 = \{x \in \mathbb{C} \mid \mathrm{Im}(x) > 0\}$. Let $(a_1, \ldots, a_n)$ and $[a_1, \ldots, a_n]$ be an ordered and unordered list of n elements allowing repetition, respectively. $(a_1^\downarrow, \ldots, a_n^\downarrow)$ stands for the ordered list obtained by sorting $[a_1, \ldots, a_n]$, $a_i \in \mathbb{C}$ such that $\mathrm{Im}(a_i^\downarrow) > \mathrm{Im}(a_j^\downarrow)$ [and $\mathrm{Re}(a_i^\downarrow) \geqslant \mathrm{Re}(a_j^\downarrow)$ if $\mathrm{Im}(a_i^\downarrow) = \mathrm{Im}(a_j^\downarrow)$] for $i < j$. We denote $\mathrm{Conf}_n(\mathbb{F})$ ($\mathrm{UConf}_n(\mathbb{F})$) as the nth-ordered (unordered) configuration space of topological space $\mathbb{F}$ ($\mathrm{Conf}_n(\mathbb{F}) = \{(m_1, \ldots, m_n) \in \mathbb{F}^n \mid m_i \neq m_j \text{ for all } i \neq j\}$). $\mathcal{B}_n$ and S_n denote the braid group on n strands and the n-order symmetric group, respectively. σ_i represents the Pauli matrix.

Consider a $\mu \times \mu$ Hamiltonian $H(\lambda)$ that depends on d-dimensional parameters $\lambda \in \mathbb{R}^d$. We focus on the following antiunitary symmetries:

$$\begin{aligned}
&\text{PT:} \quad U_{\mathrm{PT}} H^*(\lambda) U_{\mathrm{PT}}^{-1} = H(\lambda), \quad U_{\mathrm{PT}} U_{\mathrm{PT}}^* = \pm 1,\\
&\text{psH:} \quad G_{\mathrm{psH}} H^\dagger(\lambda) G_{\mathrm{psH}}^{-1} = H(\lambda),\\
&\text{CP:} \quad U_{\mathrm{CP}} H^*(\lambda) U_{\mathrm{CP}}^{-1} = -H(\lambda), \quad U_{\mathrm{CP}} U_{\mathrm{CP}}^* = \pm 1,\\
&\text{CS:} \quad G_{\mathrm{CS}} H^\dagger(\lambda) G_{\mathrm{CS}}^{-1} = -H(\lambda),
\end{aligned} \tag{1}$$

where U_s (G_s) are unitary (Hermitian) matrices and $*$ and $\dagger$ denote the complex conjugate and conjugate transpose, respectively. Based on these symmetries, we study the m-fold degeneracy points, which correspond to the m-fold multiple roots of the characteristic polynomial of $H(\lambda)$:

$$\begin{aligned}
P_\lambda(E) &= \det[H(\lambda) - E]\\
&= a_\mu(\lambda) E^\mu + \cdots + a_1(\lambda) E + a_0(\lambda).
\end{aligned} \tag{2}$$

The symmetries in Eq. (1) require that all the coefficients of Eq. (2) a_i are either real or imaginary. Thus, the codimension of a two-fold degeneracy point equals 1 in general [45] (see the Supplemental Material, Sec. I [59] for details). Consequently, it is generally impossible for a closed path in a 2D parameter space to enclose a degeneracy point without encountering any other degeneracy points, as illustrated in the right panel of Fig. 1(a) where the path (blue-black arrowed line) unavoidably passes through a line of degeneracy (purple line). Previous studies introduced the winding number of the resultant vector to address this issue [45]. However, the winding number is abelian; thus, it generally cannot capture the nonabelian topology intrinsic to non-Hermitian systems, although there may be an exceptional case where the topology is abelian.

In the main text, we primarily focus on PT symmetry. Other symmetries in Eq. (1) are investigated in the Supplemental Material, Sec. II [59]. The approach is summarized as follows: CP symmetry and CS symmetry can be mapped onto PT symmetry and psH symmetry, respectively, by transforming H to iH. Furthermore, psH symmetry can be encompassed in the subsequent discussion of PT symmetry.

For a Hamiltonian with PT symmetry, its eigenvalues are real or appear in complex conjugate pairs. We begin by assuming that, within a parameter region, the number of conjugate pairs of eigenvalues remains constant and equals m. In this case, the topological space of eigenvalues can be represented as

$$X^{(m)} = \{[\epsilon_1, \ldots, \epsilon_m, \epsilon_m^*, \ldots, \epsilon_1^*, \tilde{\epsilon}_1, \ldots, \tilde{\epsilon}_{\mu-2m}]\}, \tag{3}$$

where $\mathrm{Im}(\epsilon_i) \geqslant 0$, $\tilde{\epsilon}_i \in \mathbb{R}$, $\tilde{\epsilon}_i \neq \tilde{\epsilon}_j$ for all $i \neq j$. The unordered nature of the list arises from the equivalence of polynomials under the permutation of roots, while the condition $\tilde{\epsilon}_i \neq \tilde{\epsilon}_j$ results from the assumption that m remains constant. It is important to note that the length of the eigenvalue list does not change at exceptional points according to our definition [27]. Next, we identify the singularity within the eigenvalue space. We define the complex conjugate pair degeneracy point (CPDP) as a degeneracy point where $\epsilon_i = \epsilon_j$ and simultaneously there exist another two eigenvalues $\epsilon_i^* = \epsilon_j^*$ for $(i \neq j)$. The appearance of CPDP is a codimension 2 phenomenon (see details in the Supplemental Material, Sec. III [59]). To remove these singularities, we denote the space punctured by CPDPs as

$$X_0^{(m)} = \{(\epsilon_1^\downarrow, \ldots, \epsilon_m^\downarrow, (\epsilon_m^\downarrow)^*, \ldots, (\epsilon_1^\downarrow)^*, \tilde{\epsilon}_1^\downarrow, \ldots, \tilde{\epsilon}_{\mu-2m}^\downarrow)\}, \tag{4}$$

where $\epsilon_i^\downarrow \neq \epsilon_j^\downarrow$ for $i \neq j$ and we sorted the unordered eigenvalue list in Eq. (3), resulting in a unique representation. We define a map g from $X_0^{(m)}$ to $\mathrm{Conf}_m(\mathbb{C}_+) \times \mathrm{Conf}_{\mu-2m}(\mathbb{R})$ as follows:

$$\begin{aligned}
&g[(\epsilon_1^\downarrow, \ldots, \epsilon_m^\downarrow, (\epsilon_m^\downarrow)^*, \ldots, (\epsilon_1^\downarrow)^*, \tilde{\epsilon}_1^\downarrow, \ldots, \tilde{\epsilon}_{\mu-2m}^\downarrow)]\\
&\quad \equiv (\epsilon_1^\downarrow, \ldots, \epsilon_m^\downarrow, \tilde{\epsilon}_1^\downarrow, \ldots, \tilde{\epsilon}_{\mu-2m}^\downarrow).
\end{aligned} \tag{5}$$

The map g is injective and continuous and its inverse is also continuous. Therefore, it is a homeomorphism between $X_0^{(m)}$ and its image $g(X_0^{(m)})$:

$$\begin{aligned} X_0^{(m)} &\cong g\big(X_0^{(m)}\big) \\ &= \{(\epsilon_1^{\downarrow}, \ldots, \epsilon_m^{\downarrow}, \tilde{\epsilon}_1^{\downarrow}, \ldots, \tilde{\epsilon}_{\mu-2m}^{\downarrow})\} \\ &= \{([\epsilon_1, \ldots, \epsilon_m], [\tilde{\epsilon}_1, \ldots, \tilde{\epsilon}_{\mu-2m}])\} \\ &= \mathrm{UConf}_m(\mathbb{C}_+) \times \mathrm{UConf}_{\mu-2m}(\mathbb{R}). \end{aligned} \tag{6}$$

Consequently, we obtain the fundamental group of the punctured eigenvalue space $X_0^{(m)}$ (omitting the base point notation Q) as

$$\begin{aligned} \pi_1(X_0^{(m)}) &= \pi_1(\mathrm{UConf}_m(\mathbb{C}_+) \times \mathrm{UConf}_{\mu-2m}(\mathbb{R})) \\ &= \pi_1(\mathrm{UConf}_m(\mathbb{C}_+)) \\ &= \mathcal{B}_m, \end{aligned} \tag{7}$$

where we use the fact that $\pi_1(\mathrm{UConf}_{\mu-2m}(\mathbb{R}))$ is trivial [60,61] and $\pi_1(\mathrm{UConf}_m(\mathbb{C}_+)) = \mathcal{B}_m$ [62]. Therefore, the braid group $\mathcal{B}_m$ can be utilized to capture the eigenvalue topology, with its order being equal to the number of conjugate pairs of eigenvalues.

For the $\mathrm{PT}^2 = -1$ ($U_{\mathrm{PT}}U_{\mathrm{PT}}^* = -1$) case, we have

$$\langle\psi_r|U_{\mathrm{PT}}\mathcal{K}|\psi_r\rangle = -\langle\psi_r|U_{\mathrm{PT}}\mathcal{K}|\psi_r\rangle = 0. \tag{8}$$

Here $|\psi_r\rangle$ denotes a right eigenvector with eigenvalue ϵ, and $\mathcal{K}$ is the complex conjugate operator. This equation indicates that $|\psi_r\rangle$ and $U_{\mathrm{PT}}\mathcal{K}|\psi_r\rangle$ are linearly independent [63]. Since $U_{\mathrm{PT}}\mathcal{K}|\psi_r\rangle$ is also an eigenvector with eigenvalue ϵ^*, we conclude that $m = \mu/2$ ($m \in \mathbb{Z}$) and the number of complex conjugate pairs is equal to $\mu/2$.

For the $\mathrm{PT}^2 = 1$ case (which also includes the psH case. See Supplemental Material, Sec. II [59]), the number of complex conjugate pairs of eigenvalues [roots of the characteristic polynomial $P_\lambda(E)$] can vary. This number for a μ-order real coefficient polynomial $P_\lambda(E)$ can be characterized by $\mathbb{Z}_2^\mu$, the revised sign list of its discriminant sequence [64,65].

The revised sign list can be introduced as follows. First, we consider a polynomial p's discrimination matrix $\mathrm{Discr}(p)$. This matrix is a variant of the Sylvester matrix, defined in Eq. (S18) in the Supplemental Material, Sec. III [59]. We denote the determinant of the submatrix of $\mathrm{Discr}(p)$ formed by the first $2k$ rows and the first $2k$ columns as D_k for $k = 1, \ldots, n$. The resulting n-tuple

$$(D_1, D_2, \ldots, D_n) \tag{9}$$

is referred as the discriminant sequence of the polynomial $p(x)$. Then, the corresponding sequence

$$(\mathrm{sign}(D_1), \mathrm{sign}(D_2), \ldots, \mathrm{sign}(D_n)) \tag{10}$$

is termed the sign list of the discriminant sequence. Given a sign list $(s_1, s_2, \ldots, s_n)$, we construct a new list $(\Upsilon_1, \Upsilon_2, \ldots, \Upsilon_n)$, namely, the **revised** sign list, as follows.

(1) If a section of the given list $(s_i, s_{i+1}, \ldots, s_{i+j})$ meets the condition where $s_i \neq 0$, $s_{i+1} = s_{i+2} = \cdots = s_{i+j-1} = 0$, $s_{i+j} \neq 0$, then we replace $(s_i, s_{i+1}, \ldots, s_{i+j})$ with

$$(s_i, -s_i, -s_i, s_i, s_i, -s_i, -s_i, s_i, s_i, -s_i, \ldots,).$$

TABLE I. The number of complex conjugate pairs of eigenvalues (middle column) of a 6×6 non-Hermitian matrix exhibiting PT or psH symmetry and the corresponding possible revised sign list of the discriminant sequence (right column) is shown. The number of complex conjugate pairs equals the number of sign changes in the sign list.

Degree n	Number of complex conjugate pairs	Possible revised sign list
6	3	$(+, -, +, -, -, -)$
	2	$(+, -, +, +, +, +)$
	1	$(+, -, -, -, -, -)$
	0	$(+, +, +, +, +, +)$

Specifically, let $\Upsilon_{i+r} = (-1)^{\mathrm{floor}(\frac{r+1}{2})} \cdot s_i$ for $r = 1, 2, \ldots, j-1$. Otherwise, $\Upsilon_k = s_k$. For example, the revision of the sign list $(+, -, 0, 0, +)$ is $(+, -, +, +, +)$, where the 0s are replaced.

Now, with the revised sign list introduced, the number of complex conjugate pairs can be analyzed: it equals the number of sign changes in this revised sign list (see Theorem S1 in the Supplemental Material, Sec. III [59] and Table I). For a region with a constant number m of conjugate pairs, we can apply directly the above analysis and use the braid group $\mathcal{B}_m$ to capture the eigenvalue topology.

We proceed to consider the situation where the number of complex conjugate pairs m varies. For simplicity, we assume that $\mu = 2n$ and consider the eigenvalue space where $m = n$ or $m = n-1$ denoted as

$$X^{(n,n-1)} = \{[\epsilon_1, \ldots, \epsilon_{n-1}, \epsilon_{n-1}^*, \ldots, \epsilon_1^*, \epsilon_n, \hat{\epsilon}_n]\}, \tag{11}$$

where when $m = n$, $\hat{\epsilon}_n = \epsilon_n^*$, $\mathrm{Im}(\epsilon_i) \geqslant 0$; when $m = n-1$, $\mathrm{Im}(\hat{\epsilon}_n) = \mathrm{Im}(\epsilon_n) = 0$, $\mathrm{Im}(\epsilon_i) > 0$ and $\mathrm{Re}(\hat{\epsilon}_n) \neq \mathrm{Re}(\epsilon_n)$. So, we have $\epsilon_n \in \mathbb{C}_+$ and $\hat{\epsilon}_n \in \mathbb{C}_-$. We define the following set in $X^{(n,n-1)}$:

$$\begin{aligned} \hat{X}^{(n-1)} &= \{[\epsilon_1, \ldots, \epsilon_{n-1}, \epsilon_{n-1}^*, \ldots, \epsilon_1^*, \tilde{\epsilon}_n, \hat{\tilde{\epsilon}}_n] \\ &\qquad \times |\mathrm{Im}(\epsilon_i) > 0, \tilde{\epsilon}_n \in \mathbb{R}, \hat{\tilde{\epsilon}}_n \in \mathbb{R}\} \\ &= ((\mathbb{C}_+^0)^{n-1}/S_{n-1}) \times (\mathbb{R}^2/S_2). \end{aligned} \tag{12}$$

The eigenvalue space $X^{(n,n-1)}$ is the union of $X^{(n)}$ [defined in Eq. (3)], and $\hat{X}^{(n-1)}$. And $X^{(n)} \cap \hat{X}^{(n-1)} = \{[\epsilon_1, \ldots, \epsilon_{n-1}, \epsilon_{n-1}^*, \ldots, \epsilon_1^*, \tilde{\epsilon}_n, \tilde{\epsilon}_n] \mid \mathrm{Im}(\epsilon_i) > 0, \tilde{\epsilon}_n \in \mathbb{R}\} = [(\mathbb{C}_+^0)^{n-1}/S_{n-1}] \times \mathbb{R}$. We remove CPDPs from the eigenvalue space (denoted with the subscript 0), resulting in $X_0^{(n)} = \mathrm{UConf}_n(\mathbb{C}_+)$, $\hat{X}_0^{(n-1)} = \mathrm{UConf}_{n-1}(\mathbb{C}_+^0) \times (\mathbb{R}^2/S_2)$, and $X_0^{(n,n-1)} = X_0^{(n)} \cup \hat{X}_0^{(n-1)}$. These sets are open and path-connected due to the half-disk topology. By the Seifert–van Kampen theorem [56], the fundamental group of $X_0^{(n,n-1)}$, with $Q_0 \in X_0^{(n)} \cap \hat{X}_0^{(n-1)}$ as the base point, is isomorphic to the free product of the fundamental group of $X_0^{(n)}$, $\hat{X}_0^{(n-1)}$ with an amalgamation of $\pi_1(X_0^{(n)} \cap \hat{X}_0^{(n-1)}, Q_0)$:

$$\begin{aligned} &\pi_1\big(X_0^{(n,n-1)}, Q_0\big) \\ &\quad = \pi_1\big(X_0^{(n)}, Q_0\big) *_{\pi_1(X_0^{(n)} \cap \hat{X}_0^{(n-1)}, Q_0)} \pi_1\big(\hat{X}_0^{(n-1)}, Q_0\big) \\ &\quad = \mathcal{B}_n, \end{aligned} \tag{13}$$

where $*_{\pi_1(X_0^{(n)} \cap \hat{X}_0^{(n-1)}, Q_0)}$ denotes the amalgamation. The detailed proof of this result can be found in the Supplemental

Material, Sec. IV [59]. Therefore, we can analyze the eigenvalue topology for $\mu = 2n$ and $m \in \{n, n-1\}$. The generalization to $\mu = 2n+1$ is detailed in the Supplemental Material, Sec. V [59], where the order of the braid group is also n. Thus, these two situations can be summarized as follows: when m varies between floor$(\mu/2)$ and floor$(\mu/2)-1$, the order of the braid group n equals floor$(\mu/2)$.

In summary, CPDPs are classified by the braid group $\mathcal{B}_n$, where the order n corresponds to the number of complex conjugate pairs of eigenvalues m for both the cases of $\mathrm{PT}^2 = \pm 1$ and psH. However, in the case of $\mathrm{PT}^2 = 1$ and the corresponding psH case with m ranging from floor$(\mu/2)$ to floor$(\mu/2)-1$, the order n is floor$(\mu/2)$. We note that our results are applicable to parameter spaces with dimensions higher than 2 where CPDPs are manifest as lines.

The braid-invariant characterizing CPDP or a path can be obtained using Artin braid word [68]. We consider a directional closed path with a base point, denoted as Γ in Fig. 1(b), which encloses two CPDPs (represented by red open circles) with a base point Q_0 in a 2D parameter space. Initially, the eigenvalues are sorted as $(\epsilon_1^{\downarrow}, \epsilon_2^{\downarrow}, \ldots, \epsilon_\mu^{\downarrow})$, as shown in Fig. 1(c), and we focus on the first n eigenvalues [represented by red dots in Fig. 1(c)]. Importantly, as the eigenvalues evolve along Γ, we can consistently identify the eigenvalue strands originating from these n eigenvalues as the first n eigenvalues in the specified order. (See Supplemental Material, Sec. II [59] for more details. The defective eigenspaces of exceptional points are utilized there to identify the eigenvalue strands). For example, in Fig. 1(d), we make such identifications as indicated by the orange arrows, resulting in the first three eigenvalues being marked in red. Subsequently, we sort these n eigenvalues along Γ and denote the crossing of the ith eigenvalue over (under) the $i+1$th eigenvalue as τ_i (τ_i^{-1}), as shown in Fig. 1(d). The braid invariant of the path Γ is then given by the sequence of τ_i (τ_i^{-1}) in the order they appear along Γ [e.g., $\tau_1\tau_2^{-1}$ in Fig. 1(d)]. τ_i satisfies the braid relations [68] (see details in the Supplemental Material, Sec. VI [59]).

Examples. In this section, we present a model with PT symmetry and its circuit simulation to illustrate our theories. We confirm the occurrence of the path-dependent annihilation of CPDPs, which is brought about by the braid group, as well as an NACR that governs the behaviors of CPDPs. The NACR can be summarized as follows: for a time-varying Hamiltonian $H(\lambda(t))$ with braid topology, the braid invariants obtained from a fixed path with a fixed base point are conjugate between initial time t_i and final time t_f, as long as there is no CPDP passing through the path during this time period. This can be expressed mathematically as

$$b_\Gamma(t_f) = b_{\mathrm{dyn}}^{-1} b_\Gamma(t_i) b_{\mathrm{dyn}}, \tag{14}$$

where b_i represents an element in the braid group and b_{dyn} is a dynamical factor that acts indiscriminately [29,30,56].

We consider a six-state model described by the following Hamiltonian:

$$H = \begin{pmatrix} H_1 & \mathbb{I}_2 & 0 \\ \mathbb{I}_2 & H_2 & \Xi_1 \\ \Xi_2 & \mathbb{I}_2 & H_3 \end{pmatrix}, \tag{15}$$

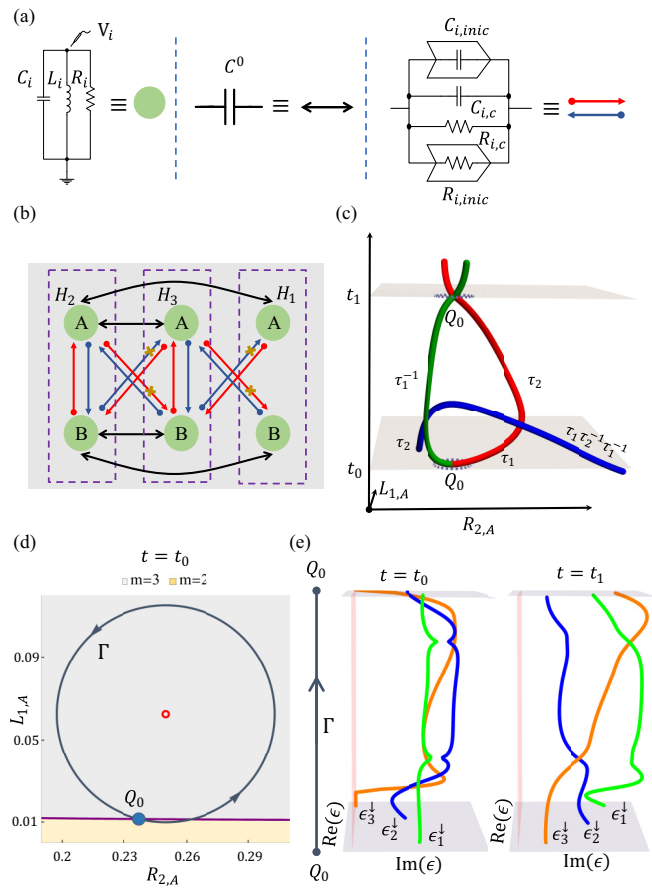

FIG. 2. (a) Electric elements used in our model: an LC-R resonant cavity as a state, the capacitor C^0 as an identical coupling, and four independently tunable elements for arbitrary coupling. $C_{i,\mathrm{inic}}$ and $R_{i,\mathrm{inic}}$ represent a negative impedance converter with current inversion (INIC) associated with a capacitor and a resistor [53,66,67], respectively. (b) The circuit, where the subsystem enclosed by the purple dashed box is equivalent to H_i in Eq. (16). (c) Path-dependent annihilation of CPDP lines in the $(R_{2,A}, L_{1,A}, t)$ space. The blue-black dashed line denotes the path Γ originating from point Q_0. (d) At $t = t_0$, the blue-black path Γ enclosing the CPDP (the red open circle), traverses two regions (gray and beige) with different numbers of conjugate pairs of eigenvalues. (e) The first *three* eigenvalue strands braiding along the path Γ in (c) at $t = t_0$ and $t = t_1$. Here the green, blue, and orange lines represent eigenvalues with decreasing imaginary parts at the beginning of Γ. Detailed parameters are provided in the Supplemental Material, Sec. VII [59] and their projective trajectories are presented in Fig. S3.

where

$$H_i = \begin{pmatrix} \omega_i + i l_i & \kappa_i \\ \kappa_i^* & \omega_i - i l_i \end{pmatrix}, \tag{16}$$

with $\omega_i, l_i \in \mathbb{R}$, $\kappa \in \mathbb{C}$. Additionally, we have $\Xi_1 = \mathbb{I}_2 + \xi(\sigma_1 - \sigma_2)$ and $\Xi_2 = p_1\sigma_1 + p_2\sigma_2$. The Hamiltonian H in Eq. (15) exhibits PT symmetry, where

$$\hat{U}_{\mathrm{PT}} = \mathbb{I}_3 \otimes \sigma_x, \quad \hat{U}_{\mathrm{PT}}\hat{U}_{\mathrm{PT}}^* = 1. \tag{17}$$

To realize this Hamiltonian, we employ the circuit system depicted in Fig. 2. In this system, $\omega_{i,A(B)}$ represents the LC resonant frequency of the $A(B)$ sublattice, and the complex

voltage $V_{i,A(B)}$ at the node of the $A(B)$ resonators corresponds to the wave function at the $A(B)$ site [left panel of Fig. 2(a)]. The gain or loss in each cavity, denoted by l_i, can be achieved using negative or positive resistors, while normal coupling is introduced with a capacitor [middle panel of Fig. 2(a)]. Arbitrary nonreciprocal coupling is achievable with INICs [right panel of Fig. 2(a)] [53,66]. Therefore, the Hamiltonian in Eq. (15) can be realized using the circuit shown in Fig. 2(b) with appropriately chosen circuit elements (see the detailed discussion in Supplemental Material, Sec. VII [59]). For example, the coupling of the circuit inside the purple dashed box in Fig. 2(b) is given by the matrix

$$\begin{pmatrix} \omega_{i,A} - \frac{i}{2C_iR_{i,A}} & \frac{i(R_{i,\mathrm{inic}}-R_{i,c})}{2C_iR_{i,\mathrm{inic}}R_{i,c}} + \omega_{i,B}\frac{C_{i,c}-C_{i,\mathrm{inic}}}{2C_i} \\ \frac{i(R_{i,\mathrm{inic}}+R_{i,c})}{2C_iR_{i,\mathrm{inic}}R_{i,c}} + \omega_{i,B}\frac{C_{i,c}+C_{i,\mathrm{inic}}}{2C_i} & \omega_{i,B} - \frac{i}{2C_iR_{i,B}} \end{pmatrix}, \tag{18}$$

which has the same form as H_i in Eq. (16).

This system exhibits the path-dependent annihilation of degeneracy points, a unique characteristic of systems with nonabelian topology [1,30]. To observe this phenomenon, we allow certain circuit parameters to vary with time while preserving PT symmetry. Figure 2(c) illustrates the evolution of CPDPs in the three-dimensional (3D) $(R_{2,A}, L_{1,A}, t)$ parameter space. At t_0, a pair of CPDPs emerges [green and red lines in Fig. 2(c)]. We associate the red CPDP with the braid word $b_{\mathrm{red}} = \tau_1$ and the green CPDP with the braid word $b_{\mathrm{green}} = \tau_1^{-1}$, both with respect to a base point Q_0. On either side of these CPDPs, there are two additional blue CPDPs associated with the braid words $b_{\mathrm{blue},l} = \tau_2$ and $b_{\mathrm{blue},r} = \tau_1\tau_2^{-1}\tau_1^{-1}$ at t_0. As depicted in Fig. 2(d), the path Γ traverses two regions with $m = 2$ and $m = 3$ conjugate pairs at $t = t_0$. Accordingly, we select the base point Q_0 on the exceptional line [purple line in Fig. 2(d)] that separates these two regions. As shown in Fig. 2(c), the red and green CPDPs subsequently deviate from their original paths and encircle the nodal line formed by the blue CPDP along the t axis. When the blue nodal line with the braid word $b_{\mathrm{blue},r}$ passes above the red nodal line, the braid invariant of the red line becomes conjugate to the blue line $\bar{b}_{\mathrm{red}} = b_{\mathrm{blue},r}^{-1} b_{\mathrm{red}} b_{\mathrm{blue},r} = \tau_2$. Additionally, there is a dynamical factor $b_{\mathrm{dyn}} = \tau_1\tau_2\tau_1\tau_2$ involved in this time evolution. According to the NACR in Eq. (14), the braid word of the path Γ at $t = t_1$ is given by $b_\Gamma(t_1) = b_{\mathrm{dyn}}^{-1}\bar{b}_{\mathrm{red}} b_{\mathrm{green}} b_{\mathrm{dyn}} = \tau_2^{-1}\tau_1$. Consequently, instead of annihilation, a third-order CPDP appears when the red and green nodal lines merge at t_1 before subsequently splitting again. As illustrated in Fig. 2(e), the braid words of the same path Γ differ at $t = t_0$ and $t = t_1$: 1 (left panel) and $\tau_2^{-1}\tau_1$ (right panel), respectively. (Detailed algebra can be found in Supplemental Material Sec. VI [59].)

The example above verifies that CPDPs follow a NACR, even when the number of conjugate pairs undergoes changes. Consequently, the braid topology governing CPDPs grants us the ability to manipulate and harness these singularities. In comparison to the case without symmetry, the merge point at $t = t_1$ exhibits two third-order degeneracies, suggesting potential applications in sensing devices [23,24,49,50]. The model with $\mathrm{PT}^2 = -1$ is provided in the Supplemental Material, Sec. VIII [59].

Conclusion and discussions. In conclusion, we provided a systematic investigation of the braid topology in non-Hermitian systems where symmetries play a crucial role in reducing the codimension of degeneracy points. Instead of relying solely on the oversimplified winding number topology [45], we uncovered the fascinating phenomenon of the path-dependent coalescence of CPDPs. The existence of the NACR under symmetries aligns with the nonabelian nature of non-Hermitian multiband eigenvalue topology [28–31], providing a more coherent picture. Moreover, the models we presented can be experimentally realized in various platforms, such as acoustic cavities [40,41], optical waveguides [69,70], and ring resonators [21,71]. These findings empower researchers in diverse fields to harness symmetry in non-Hermitian systems, leading to significant implications and inspiring further investigations into symmetry-protected non-Hermitian degeneracy points and their applications.

Note added. We become aware of a parallel work [72] which overlaps with parts of this work.

Acknowledgments. This work was supported by the National Key Research and Development Program of China (Grant No. 2022YFA1404900), the National Natural Science Foundation of China (Grants No. 12274330 and No. 12274332), and the Knowledge Innovation Program of Wuhan-Shuguang (Grant No. 2022010801020125).

[1] Q. Wu, A. A. Soluyanov, and T. Bzdušek, Science **365**, 1273 (2019).
[2] C. Fang, Y. Chen, H.-Y. Kee, and L. Fu, Phys. Rev. B **92**, 081201(R) (2015).
[3] T. Bzdušek and M. Sigrist, Phys. Rev. B **96**, 155105 (2017).
[4] C. Fang, H. Weng, X. Dai, and Z. Fang, Chin. Phys. B **25**, 117106 (2016).
[5] N. P. Armitage, E. J. Mele, and A. Vishwanath, Rev. Mod. Phys. **90**, 015001 (2018).
[6] M. Z. Hasan, G. Chang, I. Belopolski, G. Bian, S.-Y. Xu, and J.-X. Yin, Nat. Rev. Mater. **6**, 784 (2021).
[7] B. Yan and C. Felser, Annu. Rev. Condens. Matter Phys. **8**, 337 (2017).
[8] A. A. Soluyanov, D. Gresch, Z. Wang, Q. Wu, M. Troyer, X. Dai, and B. A. Bernevig, Nature (London) **527**, 495 (2015).
[9] L. Xu, H.-X. Wang, Y.-D. Xu, H.-Y. Chen, and J.-H. Jiang, Opt. Express **24**, 18059 (2016).
[10] X. Zhang, H.-X. Wang, Z.-K. Lin, Y. Tian, B. Xie, M.-H. Lu, Y.-F. Chen, and J.-H. Jiang, Nat. Phys. **15**, 582 (2019).
[11] H. Jia, R. Zhang, W. Gao, Q. Guo, B. Yang, J. Hu, Y. Bi, Y. Xiang, C. Liu, and S. Zhang, Science **363**, 148 (2019).
[12] I. Sodemann and L. Fu, Phys. Rev. Lett. **115**, 216806 (2015).
[13] M. Ünzelmann, H. Bentmann, T. Figgemeier, P. Eck, J. N. Neu, B. Geldiyev, F. Diekmann, S. Rohlf, J. Buck, M. Hoesch, M. Kalläne, K. Rossnagel, R. Thomale, T. Siegrist, G. Sangiovanni, D. D. Sante, and F. Reinert, Nat. Commun. **12**, 3650 (2021).

[14] A. Bouhon, Q. Wu, R.-J. Slager, H. Weng, O. V. Yazyev, and T. Bzdušek, Nat. Phys. **16**, 1137 (2020).
[15] Q. Guo, T. Jiang, R.-Y. Zhang, L. Zhang, Z.-Q. Zhang, B. Yang, S. Zhang, and C. T. Chan, Nature (London) **594**, 195 (2021).
[16] K. Kawabata, K. Shiozaki, M. Ueda, and M. Sato, Phys. Rev. X **9**, 041015 (2019).
[17] K. Kawabata, T. Bessho, and M. Sato, Phys. Rev. Lett. **123**, 066405 (2019).
[18] E. J. Bergholtz, Rev. Mod. Phys. **93**, 015005 (2021).
[19] K. Ding, C. Fang, and G. Ma, Nat. Rev. Phys. **4**, 745 (2022).
[20] M.-A. Miri and A. Alù, Science **363**, eaar7709 (2019).
[21] K. Wang, A. Dutt, C. C. Wojcik, and S. Fan, Nature (London) **598**, 59 (2021).
[22] S. Sayyad, M. Stalhammar, L. Rodland, and F. K. Kunst, SciPost Phys. **15**, 200 (2023).
[23] H. Hodaei, A. U. Hassan, S. Wittek, H. Garcia-Gracia, R. El-Ganainy, D. N. Christodoulides, and M. Khajavikhan, Nature (London) **548**, 187 (2017).
[24] K. Bai, J.-Z. Li, T.-R. Liu, L. Fang, D. Wan, and M. Xiao, Phys. Rev. Lett. **130**, 266901 (2023).
[25] H. Nasari, G. Lopez-Galmiche, H. E. Lopez-Aviles, A. Schumer, A. U. Hassan, Q. Zhong, S. Rotter, P. LiKamWa, D. N. Christodoulides, and M. Khajavikhan, Nature (London) **605**, 256 (2022).
[26] S. Sayyad, Phys. Rev. Res. **4**, 043213 (2022).
[27] Y. Ashida, Z. Gong, and M. Ueda, Adv. Phys. **69**, 249 (2020).
[28] C. C. Wojcik, X.-Q. Sun, T. Bzdušek, and S. Fan, Phys. Rev. B **101**, 205417 (2020).
[29] Z. Li and R. S. K. Mong, Phys. Rev. B **103**, 155129 (2021).
[30] C.-X. Guo, S. Chen, K. Ding, and H. Hu, Phys. Rev. Lett. **130**, 157201 (2023).
[31] H. Hu, S. Sun, and S. Chen, Phys. Rev. Res. **4**, L022064 (2022).
[32] J. L. K. König, K. Yang, J. C. Budich, and E. J. Bergholtz, Phys. Rev. Res. **5**, L042010 (2023).
[33] H. Kedia, I. Bialynicki-Birula, D. Peralta-Salas, and W. T. M. Irvine, Phys. Rev. Lett. **111**, 150404 (2013).
[34] E. Pisanty, G. J. Machado, V. Vicuña-Hernández, A. Picón, A. Celi, J. P. Torres, and M. Lewenstein, Nat. Photon. **13**, 569 (2019).
[35] J. Leach, M. R. Dennis, J. Courtial, and M. J. Padgett, Nature (London) **432**, 165 (2004).
[36] C. H. Lee, A. Sutrisno, T. Hofmann, T. Helbig, Y. Liu, Y. S. Ang, L. K. Ang, X. Zhang, M. Greiter, and R. Thomale, Nat. Commun. **11**, 4385 (2020).
[37] X.-Q. Sun, B. Lian, and S.-C. Zhang, Phys. Rev. Lett. **119**, 147001 (2017).
[38] E. Witten, Commun. Math. Phys. **121**, 351 (1989).
[39] R.-J. Slager, A. Bouhon, and F. N. Ünal, arXiv:2208.12824.
[40] Q. Zhang, Y. Li, H. Sun, X. Liu, L. Zhao, X. Feng, X. Fan, and C. Qiu, Phys. Rev. Lett. **130**, 017201 (2023).
[41] Q. Zhang, L. Zhao, X. Liu, X. Feng, L. Xiong, W. Wu, and C. Qiu, Phys. Rev. Res. **5**, L022050 (2023).
[42] Y. Yu, L.-W. Yu, W. Zhang, H. Zhang, X. Ouyang, Y. Liu, D.-L. Deng, and L.-M. Duan, npj Quantum Inf. **8**, 116 (2022).
[43] A. P. Schnyder, Phys. Rev. B **78**, 195125 (2008).
[44] A. Melkani, Phys. Rev. Res. **5**, 023035 (2023).
[45] P. Delplace, T. Yoshida, and Y. Hatsugai, Phys. Rev. Lett. **127**, 186602 (2021).
[46] M. Stålhammar and E. J. Bergholtz, Phys. Rev. B **104**, L201104 (2021).
[47] R.-Y. Zhang, X. Cui, W.-J. Chen, Z.-Q. Zhang, and C. T. Chan, Commun. Phys. **6**, 169 (2023).
[48] I. Mandal and E. J. Bergholtz, Phys. Rev. Lett. **127**, 186601 (2021).
[49] K. Bai, L. Fang, T.-R. Liu, J.-Z. Li, D. Wan, and M. Xiao, Natl. Sci. Rev. **10**, nwac259 (2023).
[50] Z. Xiao, H. Li, T. Kottos, and A. Alù, Phys. Rev. Lett. **123**, 213901 (2019).
[51] R. Kononchuk, J. Cai, F. Ellis, R. Thevamaran, and T. Kottos, Nature (London) **607**, 697 (2022).
[52] C. Wang, W. R. Sweeney, A. D. Stone, and L. Yang, Science **373**, 1261 (2021).
[53] J. Hu, R.-Y. Zhang, Y. Wang, X. Ouyang, Y. Zhu, H. Jia, and C. T. Chan, Nat. Phys. **19**, 1098 (2023).
[54] S. Sayyad and F. K. Kunst, Phys. Rev. Res. **4**, 023130 (2022).
[55] H. Jia, R.-Y. Zhang, J. Hu, Y. Xiao, Y. Zhu, and C. T. Chan, Commun. Phys. **6**, 293 (2023).
[56] A. Hatcher, *Algebraic Topology* (Cambridge University Press, Cambridge, England, 2002).
[57] Y. Choi, C. Hahn, J. W. Yoon, and S. H. Song, Nat. Commun. **9**, 2182 (2018).
[58] Ş. K. Özdemir, S. Rotter, F. Nori, and L. Yang, Nat. Mater. **18**, 783 (2019).
[59] See Supplemental Material at http://link.aps.org/supplemental/10.1103/PhysRevB.109.L041102 for details, which includes Refs. [49,50,53,56,60,61,64–68,73–79].
[60] C. A. I. Zapata, arXiv:1710.00293.
[61] B. Knudsen, arXiv:1803.11165.
[62] L. Plachta, Eur. J. Math. **6**, 132 (2020).
[63] R. A. Horn and C. R. Johnson, *Matrix Analysis*, 2nd ed., corrected reprint ed. (Cambridge University Press, New York, 2017).
[64] S. Liang and J. Zhang, Sci. China E: Technol. Sci. **42**, 113 (1999).
[65] L. Yang, X. Hou, and Z. Zeng, Sci. China-Technol. Sci. **39**, 628 (1996).
[66] T. Helbig, T. Hofmann, S. Imhof, M. Abdelghany, T. Kiessling, L. W. Molenkamp, C. H. Lee, A. Szameit, M. Greiter, and R. Thomale, Nat. Phys. **16**, 747 (2020).
[67] T. Hofmann, T. Helbig, C. H. Lee, M. Greiter, and R. Thomale, Phys. Rev. Lett. **122**, 247702 (2019).
[68] C. Kassel and V. G. Turaev, *Braid Groups*, Graduate Texts in Mathematics Vol. 247 (Springer, New York, NY, 2008).
[69] J. Doppler, A. A. Mailybaev, J. Böhm, U. Kuhl, A. Girschik, F. Libisch, T. J. Milburn, P. Rabl, N. Moiseyev, and S. Rotter, Nature (London) **537**, 76 (2016).
[70] N. X. A. Rivolta and B. Maes, Opt. Lett. **40**, 3922 (2015).
[71] K. Wang, A. Dutt, K. Y. Yang, C. C. Wojcik, J. Vučković, and S. Fan, Science **371**, 1240 (2021).
[72] K. Yang, Z. Li, J. L. K. König, L. Rødland, M. Stålhammar, and E. J. Bergholtz, arXiv:2309.14416.
[73] S. Basu, R. Pollack, and M.-F. Roy, *Algorithms in Real Algebraic Geometry*, 2nd ed., Algorithms and Computation in Mathematics Vol. 10 (Springer, Berlin, 2006).
[74] A. J. Berrick, F. R. Cohen, E. Hanbury, Y.-L. Wong, and J. Wu, *Braids: Introductory Lectures on Braids, Configurations and Their Applications*, Lecture Notes Series, Institute for

Mathematical Sciences, National University of Singapore (World Scientific, Singapore, 2009), Vol. 19.

[75] *The Circuits and Filters Handbook. Feedback, Nonlinear, and Distributed Circuits*, 3rd ed., edited by W.-K. Chen (CRC Press, Boca Raton, FL, 2009).

[76] I. M. Gel'fand, M. M. Kapranov, and A. V. Zelevinsky, *Discriminants, Resultants, and Multidimensional Determinants*, Modern Birkhäuser Classics, (Birkhäuser, Boston, 2008).

[77] M. S. Dresselhaus, G. Dresselhaus, and A. Jorio, *Group Theory: Application to the Physics of Condensed Matter* (Springer, Berlin, 2010).

[78] B. C. Hall, *Lie Groups, Lie Algebras, and Representations: An Elementary Introduction*, 2nd ed., Graduate Texts in Mathematics Vol. 222 (Springer, Cham, Germany, 2015).

[79] R. Zhang, H. Qin, and J. Xiao, J. Math. Phys. **61**, 012101 (2020).